AMERICAN SOCIETY FOR MICROBIOLOGY | Journal of Virology®

GENETIC DIVERSITY AND EVOLUTION

Mammalian Orthoreovirus Reassortment Proceeds with Little Constraint on Segment Mixing

Megan R. Hockman,[a] Nathan T. Jacobs,[a] Bernardo A. Mainou,[b]* Katia Koelle,[c] Anice C. Lowen[a]

[a]Department of Microbiology and Immunology, Emory University School of Medicine, Atlanta, Georgia, USA
[b]Department of Pediatrics, Emory University School of Medicine, Atlanta, Georgia, USA
[c]Department of Biology, Emory College of Arts and Sciences, Atlanta, Georgia, USA

ABSTRACT Segmentation of viral genomes provides the potential for genetic exchange within coinfected cells. However, for this potential to be realized, coinfecting genomes must mix during the viral life cycle. The efficiency of reassortment, in turn, dictates its potential to drive evolution. The opportunity for mixing within coinfected cells may vary greatly across virus families, such that the evolutionary implications of genome segmentation differ as a result of core features of the viral life cycle. To investigate the relationship between viral replication compartments and genetic exchange, we quantified reassortment in mammalian orthoreovirus (reovirus). Reoviruses carry a 10-segmented, double-stranded RNA genome, which is replicated within proteinaceous structures termed inclusion bodies. We hypothesized that inclusions impose a barrier to reassortment. We quantified reassortment between wild-type (*wt*) and variant (*var*) reoviruses that differ by one nucleotide per segment. Studies of *wt/var* systems in both T1L and T3D backgrounds revealed frequent reassortment without bias toward particular genotypes. However, reassortment was more efficient in the T3D serotype. Since T1L and T3D viruses exhibit different inclusion body morphologies, we tested the impact of this phenotype on reassortment. In both serotypes, reassortment levels did not differ by inclusion morphology. Reasoning that the merging of viral inclusions may be critical for genome mixing, we then tested the effect of blocking merging. Reassortment proceeded efficiently even under these conditions. Our findings indicate that reovirus reassortment is highly efficient despite the localization of many viral processes to inclusion bodies, and that the robustness of this genetic exchange is independent of inclusion body structure and fusion.

IMPORTANCE Quantification of reassortment in diverse viral systems is critical to elucidate the implications of genome segmentation for viral evolution. In principle, genome segmentation offers a facile means of genetic exchange between coinfecting viruses. In practice, there may be physical barriers within the cell that limit the mixing of viral genomes. Here, we tested the hypothesis that localization of the various stages of the mammalian orthoreovirus life cycle within cytoplasmic inclusion bodies compartmentalizes viral replication and limits genetic exchange. Contrary to this hypothesis, our data indicate that reovirus reassortment occurs readily within coinfected cells and is not strongly affected by the structure or dynamics of viral inclusion bodies. We conclude that the potential for reassortment to contribute to reovirus evolution is high.

KEYWORDS genetic exchange, inclusion bodies, mammalian orthoreovirus, reassortment, reovirus, segmentation

Mammalian orthoreovirus (reovirus) is a member of the *Reoviridae* family with a 10-segmented double-stranded RNA (dsRNA) genome. The segmented nature of its genome gives rise to the potential for reassortment, the process by which segments from coinfecting parental viruses are exchanged and packaged together to yield progeny bearing novel genotypes. Along with mutation, reassortment is an important

Editor Colin R. Parrish, Cornell University

Address correspondence to Anice C. Lowen, anice.lowen@emory.edu.

*Present address: Bernardo A. Mainou, Centers for Disease Control and Prevention, Atlanta, GA, USA.

The authors declare no conflict of interest.

Received 24 October 2021
Accepted 13 December 2021
Accepted manuscript posted online 22 December 2021
Published 23 February 2022

source of genetic diversity, making its potential implications for viral evolution great. Reassortment can bring together beneficial mutations from genetically distinct parental viruses, relieving clonal interference and resulting in progeny with enhanced fitness (1, 2). Similarly, reassortment allows the purging of deleterious mutations that could otherwise prevent positive selection from acting on advantageous mutations elsewhere in the genome (3, 4). Cumulatively, reassortment allows selection to act more efficiently and can thereby enable the evolution of viruses with enhanced replicative potential, an expanded host range, or more efficient immune avoidance mechanisms.

A comprehensive understanding of the implications of reassortment for viral evolution depends on an understanding of how readily it occurs during viral coinfection. Influenza A virus reassortment is highly efficient due to a reliance on coinfection for productive replication (5–7). Furthermore, the influenza A virus life cycle appears to allow free segment mixing within coinfected cells, which may facilitate complementation and reassortment. Unlike influenza A virus, reovirus replicates within virus-derived inclusion bodies (inclusions) (8–10) that may impose a physical barrier to segment mixing. Examination of reovirus reassortment, therefore, presents an opportunity to broaden our understanding of the relationship between viral genome segmentation and diversification through genetic exchange. Barriers to viral mixing within the cell may strongly limit reassortment and, in turn, minimize the impact of genome segmentation on viral evolution.

Reovirus replication occurs within the host cell cytoplasm, with much of the life cycle confined to proteinaceous viral inclusions (11). The μNS protein is a major structural component of inclusions: expression of this protein alone is sufficient for the formation of inclusion-like objects. However, more complex structures are formed in the context of infection, with the recruitment of many viral and cellular components to inclusion bodies (12–16). Of note, rough endoplasmic reticulum membranes and ribosomes are recruited, which may remove the need for viral mRNAs to enter the cytoplasm to be translated. Translation of viral mRNA has been observed at the periphery of viral inclusions (15, 17, 18).

In most serotypes, viral inclusions exhibit filamentous morphology due to interactions between the viral μ2 protein and the host cell microtubule network. Additional interactions between μ2 and the inclusion-forming μNS protein lead to the characteristic filamentous inclusion morphology, which co-localizes with microtubules (8, 9, 19). In contrast, the T3D serotype generates globular inclusions due to a single point mutation in the μ2 gene resulting in a serine substitution at position 208 (P208S) (9). This amino acid change abrogates μ2's interaction with microtubules and causes more frequent misfolding and ubiquitination of the μ2 protein (20).

Reovirus inclusions coalesce during infection (21, 22). Inclusions in another dsRNA virus, infectious bursal disease virus, also merge together over time, and this process has been shown to yield mixed inclusion bodies within coinfected cells (23). If viral mRNAs are sequestered within inclusions (14), merging may serve as a primary source of genetic exchange. It is not known whether inclusion morphology (dictated by the μ2 protein) plays a role in segment movement. T1L and T3D viruses represent tractable systems in which to explore this possibility, as a single point mutation is sufficient to change their inclusion morphology from globular to filamentous, and *vice versa*.

Here, we sought to quantify reovirus reassortment and to evaluate the role of viral inclusions in determining reassortment frequency. Reovirus reassortment was quantified in a previously developed fitness-neutral system which uses homologous parental strains (24). To compare baseline reassortment frequencies between serotypes, reassortment was quantified in both the T1L and the T3D viruses. Reassortment was efficient in both systems, but more so in T3D. The impact of inclusion morphology was also investigated in each serotype. Alteration of inclusion morphology to either globular (in the T1L system) or filamentous (in the T3D system) had a minimal impact on reassortment, indicating that morphology is not an important determinant of genetic exchange. To investigate the role of inclusion merging in reassortment, cells were treated with nocodazole, which has been shown to block the fusion of inclusions (22).

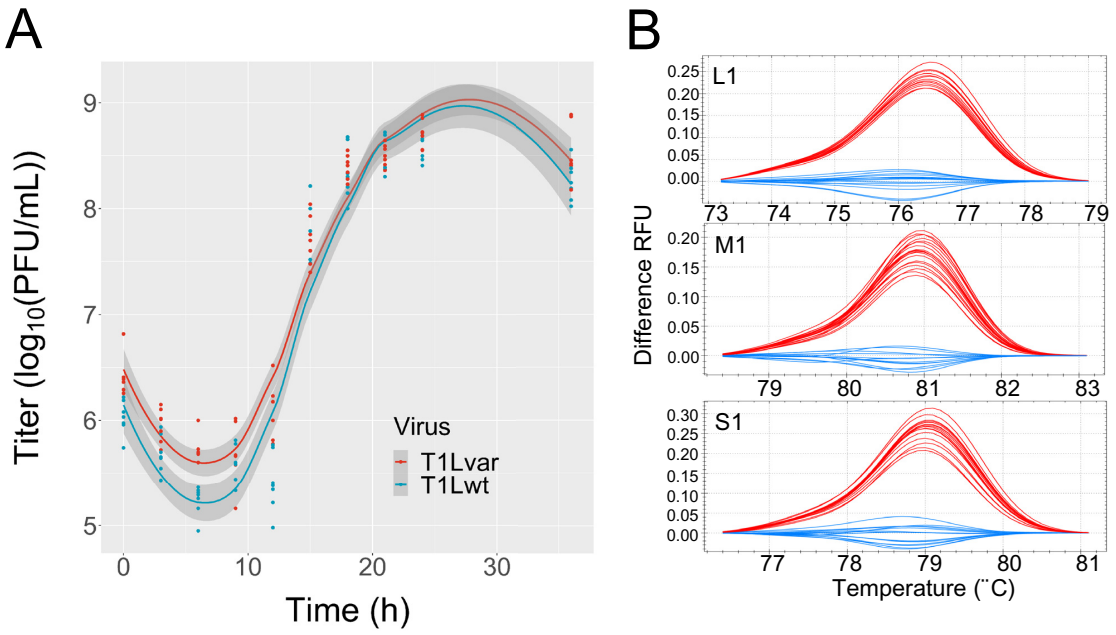

FIG 1 T1L *wt* and *var* replicate to equivalent titers and can be differentiated using high-resolution melt analysis. Single-cycle replication of T1L *wt* and *var* viruses was evaluated over a period of 36 h. Infections were performed at an MOI of 5 PFU/cell (panel A). Plaques from this time course were then genotyped using high-resolution melt analysis. Melt curves were generated for each segment and compared to *wt* and *var* controls. Representative melt curves are shown for the L1, M1, and S1 segments, with blue lines representing *wt* segments and red lines representing *var* segments (panel B). Difference in relative fluorescent units (RFU) is indicated on the *y* axis.

Reassortment levels were not markedly affected by nocodazole treatment, suggesting that inclusion merging plays a minimal role in facilitating genetic exchange.

RESULTS

Quantification of reovirus reassortment. Reassortment between divergent viruses often leads to the production of attenuated progeny due to incompatibilities between genome segments and/or proteins from different parental viruses (25). Decreased fitness may cause these progeny to be removed from the population by negative selection, leading to underrepresentation of reassortment frequencies. To quantify reassortment in the absence of segment mismatch, we designed well-matched parental viruses for coinfection. We reported this method previously (24, 26) and have applied it here to both T1L and T3D serotypes. Briefly, silent point mutations were introduced into each wild-type (*wt*) virus to generate a variant (*var*) strain that differs from *wt* by one nucleotide per gene segment (see Materials and Methods). We previously showed that there is no significant difference in the replicative fitness of T3D*wt* and T3D*var* in cell culture (24). Equivalent analysis was performed here in the T1L system: T1L*wt* and T1L*var* exhibited equivalent titers over the course of a 36-h infection (Fig. 1A). These results confirm that the genotypically similar *wt* and *var* viruses are also phenotypically comparable, as intended. Owing to the silent nature of the mutations introduced, we expect this phenotypic similarity between parental viruses to extend to reassortant progeny. To ensure that a single-nucleotide polymorphism was sufficient to distinguish the gene segments of *wt* and *var* viruses, high-resolution melt analysis was performed on reverse transcription-quantitative PCR (qRT-PCR) amplicons of the viral RNAs. In this approach, amplicons are heated gradually in the presence of a double-strand intercalating dye, such as EvaGreen. This gradual heating allows precise measurement of the amplicon's melting point, the temperature at which the amplicon separates into two DNA strands (27). The melting properties of each *var* segment differed from its

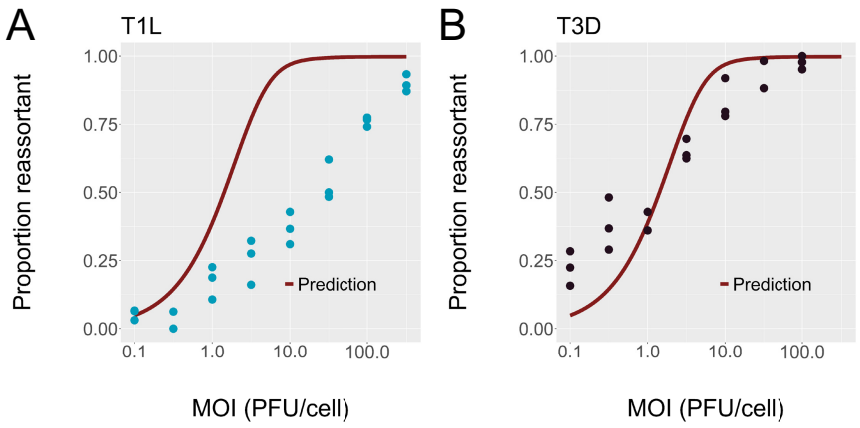

FIG 2 Reovirus reassortment occurs frequently at high MOI and is more efficient in T3D than in T1L. Reassortment between *wt* and *var* forms of the T1L (panel A) and T3D (panel B) strains of reovirus was quantified at a range of MOIs. Infections were performed in triplicate at each MOI. The proportion of progeny with any reassortant genotype is plotted against the MOI (PFU/cell). Experimental data are compared to a theoretical prediction that assumes random distribution of virus particles across cells and perfectly efficient mixing of gene segments in infected cells.

corresponding *wt* segment, indicating that the introduced polymorphisms were sufficient to identify the parental origin of each segment (Fig. 1B; [24]).

To quantify reassortment in each background, *wt* and *var* viruses were mixed in equal proportions and diluted to a range of virion concentrations. L929 cells, mouse fibroblast cells that are highly permissive to reovirus infection, were inoculated under synchronized, single-cycle conditions. Synchronization is achieved by allowing viruses to attach at 4°C before triggering entry by warming to 37°C; this process narrows the timeframe in which infection occurs such that coinfections are essentially simultaneous. Single cycle conditions prevent the propagation of viral progeny arising from the initial inoculation; this, in turn, ensures that viruses sampled are direct progeny of the parental *wt* and *var* viruses. At 24 h postinoculation (hpi), progeny viruses were collected for genotyping of clonal isolates and analysis of reassortment frequencies. The resultant data in the T1L (Fig. 2A) and T3D (Fig. 2B) backgrounds revealed that reassortment increased with increasing MOI and reached high levels, with greater than 80% of progeny carrying reassortant genotypes at the highest MOIs tested. To more formally assess reassortment efficiency, we compared the observed results to the prediction of a simple theoretical model which assumes random distribution of viruses across cells and perfectly random mixing of segments within coinfected cells. Observed T3D reassortment was similar to model predictions, consistent with robust segment exchange in coinfected cells. However, observed T1L reassortment was less efficient than predicted by the model and significantly less efficient than that of T3D ($P = 0.0009$, mixed-effects analysis).

Reovirus segments assort randomly in coinfected cells. Quantification of the proportion of progeny that are reassortant (as reported above) is informative of the efficiency of segment mixing, but does not exclude the possibility that interactions between segments may bias reassortment toward the production of particular genotypes. To determine whether interactions between segments favor the production of certain reassortant genotypes over others, we quantified pairwise associations between segments. The pairwise associations (indicated by r^2) are a measure of segment linkage, with high r^2 values indicating that the two segments considered are found together in the same virus more often than would be expected by chance. If frequencies of viral coinfection and segment mixing are high, reassortment can break segment linkage; however, even under conditions conducive to reassortment, physical or functional interactions between segments may constrain this process and lead to the maintenance of linkage. Because the coinfecting viral genomes of *wt* and *var* viruses are highly homologous, we predicted that segment exchange would occur without genetic constraint.

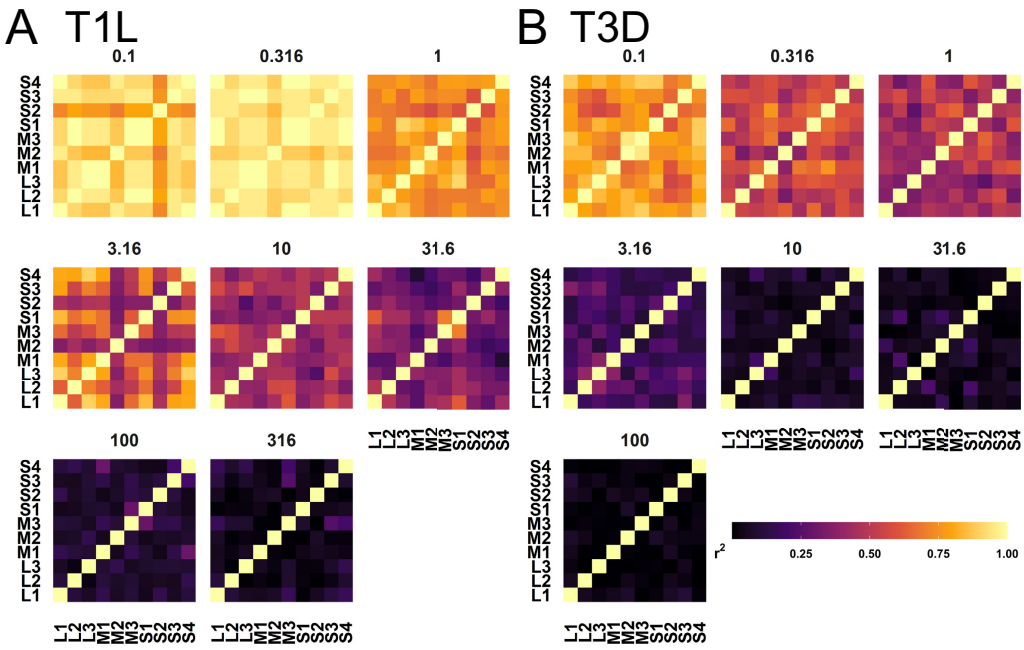

FIG 3 Under high MOI conditions, there is little pairwise association between gene segments. Genotypes of progeny viruses sampled from *wt*/*var* coinfections were analyzed to quantify pairwise associations between segments. r^2 values indicating the extent of linkage between segments are shown. Each genome segment is shown on both the *x* and *y* axes, with blocks of color indicating the magnitude of r^2. Higher r^2 values indicate an increased probability that both genome segments in a clonal isolate share the same parental genotype. Yellow coloration indicates a strong association, while purple indicates a weak or absent association. Results from coinfections with T1L *wt* and *var* (panel A), or with T3D *wt* and *var* (panel B), are shown for each MOI (indicated above each plot in units of PFU/cell).

To test our prediction, the genotypes of progeny from each viral population were analyzed to quantify pairwise associations between segments at each MOI. Specifically, r^2 was calculated for each pair of segments (e.g., M2 and S3) to quantify the extent to which both segments were derived from the same parental strain (Fig. 3). A high r^2 value, indicated by light coloration in Fig. 3, is indicative of segment linkage. Under low MOI conditions, segments remained linked due to infrequent coinfection. Importantly, at high MOIs, when coinfection is expected to be common, segments derived from a given parental strain cooccurred with segments from either parent at roughly equal frequencies, and r^2 values were therefore low. This result indicates a lack of pairwise association between segments under conditions where reassortment is abundant. We note that the transition from high to low linkage is seen at lower MOIs for T3D viruses compared to T1L. This observation is in line with the higher reassortment efficiency noted above for the T3D serotype. Overall, this analysis indicates that, when considering homologous coinfecting viruses, reovirus reassortment breaks genetic linkages among the 10 gene segments in an unbiased manner. Given these data, we conclude that segments are assorted independently, a result which is consistent with previous findings using temperature-sensitive reovirus mutants (28).

Inclusion morphology has minimal impact on reassortment. Based on the observation that reassortment is more efficient in T3D than in T1L viruses, we hypothesized that globular inclusions (like those of T3D) are more conducive to segment mixing within the cell than filamentous inclusions (like those of T1L). We reasoned that viral inclusions are likely to impose physical barriers to segment mixing, reducing the efficiency of reassortment relative to a cellular infection in which segments mix freely without physical barriers. Furthermore, inclusions that differ in structure could vary in their capacities for restricting reassortment. To directly test the impact of inclusion morphology, reassortment efficiency was quantified in both reovirus serotypes using targeted mutants designed to alter inclusion morphology. Consistent with most reovirus serotypes, the T1L virus generates filamentous inclusion bodies which have been

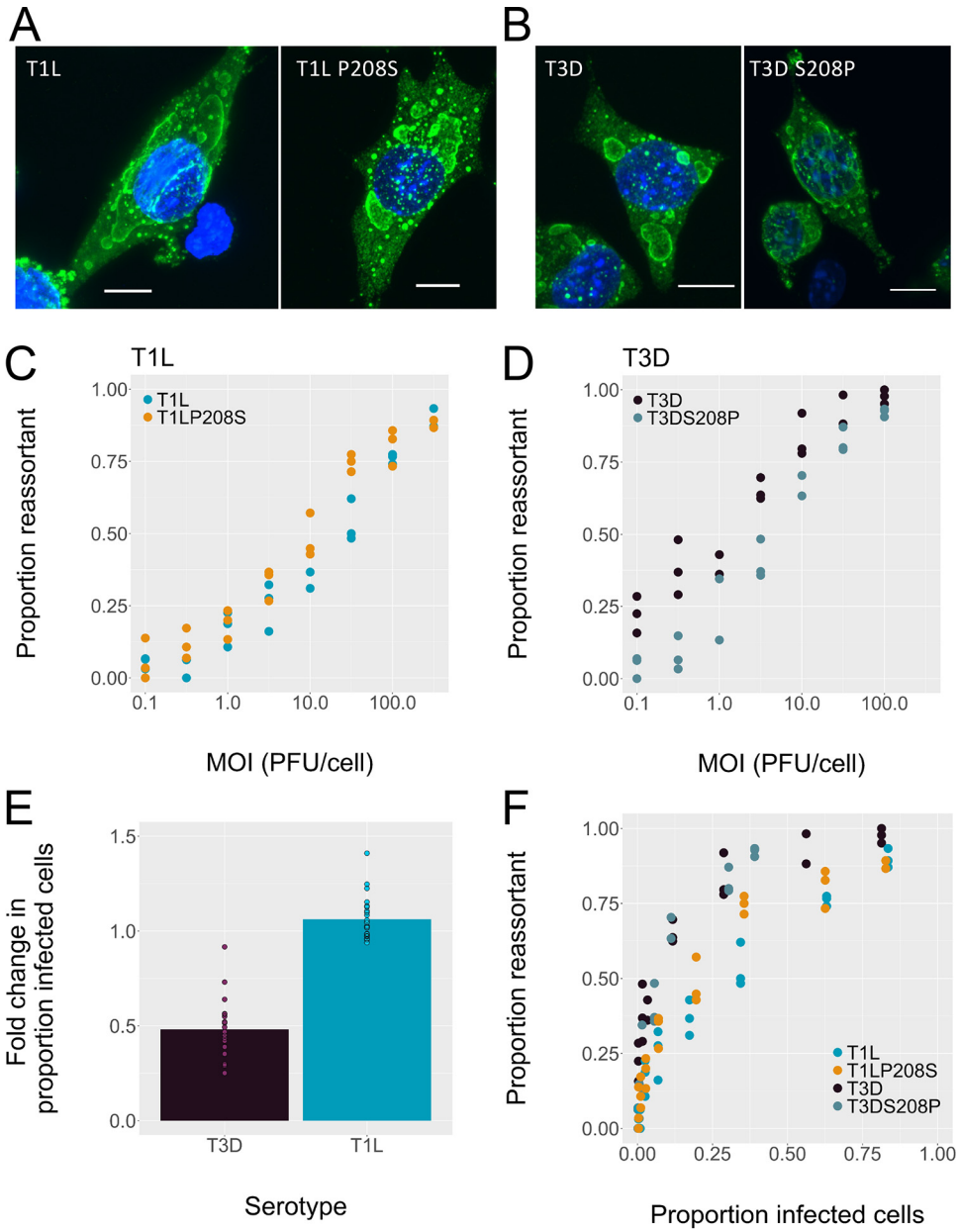

FIG 4 Reassortment efficiency is not strongly modulated by inclusion morphology. (A, B) The morphology of cytoplasmic inclusions formed by wild-type viruses and those with altered amino acid identities at μ2 position 208 was characterized by confocal microscopy, staining for nuclei (blue) and viral σNS protein (green). Filamentous T1L inclusions are changed to a globular morphology with the introduction of μ2 P208S (panel A). The converse is observed with T3D and T3D μ2 S208P (panel B). Projections from a Z stack are shown. Scale bars, 10 μm. (C, D) Reassortment was quantified for the globular T1LP208S (panel C) and filamentous T3DS208P (panel D) viruses, and plotted together with data shown in Fig. 2 for filamentous T1L and globular T3D, respectively. (E) The fold change in the proportion of cells positive for σ3 is plotted, comparing inoculation with mutant virus (T1LP208S and T3DS208P) to inoculation with wild-type virus (T1L and T3D) at a given MOI. Data points indicate fold change values observed at each MOI and bars show the mean across all MOIs. (F) Reassortment data from panels C and D are replotted against the proportion of cells expressing viral σ3 protein.

shown to co-localize with the microtubule network (19). We confirmed that this morphology was adopted using confocal microscopy (Fig. 4A). A single amino acid change of P208S in the μ2 protein abrogates its interaction with microtubules, resulting in the formation of globular inclusion bodies (9). The generation of a T1L virus bearing this polymorphism successfully altered inclusion morphology (Fig. 4A). The converse mutation was introduced in T3D, which normally forms globular inclusions. The inclusion

morphologies of T3D (globular) and T3DS208P (filamentous) were confirmed using confocal microscopy (Fig. 4B).

Reassortment frequencies did not appreciably differ between T1L and T1LP208S (Fig. 4C). A significant *P* value of 0.0004 was found at an MOI of 31.6 PFU/cell, but comparison of reassortment frequency at all other MOIs yielded nonsignificant *P* values, ranging from 0.13 to 0.99 (Sidak's multiple-comparison test). T3DS208P, which formed filamentous inclusions, exhibited consistently lower levels of reassortment compared to its globular counterpart T3D (Fig. 4D). Comparison of MOIs of 0.1 PFU/cell to 10 PFU/cell yielded significant *P* values, ranging from 0.0001 to 0.015. There was no significant difference noted between T3D and T3DS208P reassortment at 31.6 and 100 PFU/cell (Sidak's multiple-comparison test). Therefore, changing T3D inclusions from globular to filamentous moderately suppressed reassortment, but the converse change in T1L did not increase reassortment as hypothesized. Given these inconsistent outcomes, we reasoned that inclusion morphology may not be a primary determinant of reassortment efficiency. Rather, mutation of μ2 position 208 may have differentially affected virus infectivity in the T1L and T3D backgrounds, in turn altering reassortment at comparable multiplicities of infection.

To evaluate the infectivity of the viruses tested, coinfected cells stained for the viral structural protein σ3 were analyzed by flow cytometry. The T1L wild-type and μ2 mutant viruses showed comparable levels of infection, with the P208S mutation causing a 1.06-fold increase in the proportion of cells infected. Notably, however, the S208P mutation in the T3D background had a marked effect on infectivity, leading to a 0.48-fold change in the proportion of cells infected (Fig. 4E).

To determine the contribution of infectivity, rather than inclusion morphology, to observed differences in reassortment between T3D and T3DS208P, we evaluated the proportion of reassortant progeny viruses relative to the proportion of cells infected (Fig. 4F). When analyzed in this way, reassortment levels observed for T3D and T3DS208P were similar. Comparison of T1L and T1LP208S reassortment using this approach also showed little difference. Thus, at a given level of infection, filamentous and globular variants of a given serotype display comparable levels of reassortment. We therefore conclude that the frequency of reassortment in reovirus infected cells is not strongly modulated by inclusion morphology.

Efficiency of reovirus infection. To better understand the relationship between MOI and infectivity, the σ3-positive cell population was analyzed as a function of MOI. The Poisson expectation for the proportion of cells infected was used as a baseline for comparison and, relative to this expectation, all viruses exhibited markedly lower levels of infection (Fig. 5A).

The disparity between observed and expected infection levels at a given MOI raised the possibility that not all virus particles successfully reach cells during the attachment period. To address this possibility, we conducted a series of infections across a range of MOIs, and quantified unattached viruses remaining in the liquid inoculum at the end of the attachment period. Specifically, remaining liquid inoculum was pooled with washes performed following attachment, and viruses in the resultant pools were titered by plaque assay. The average proportion of inoculum virus detected in this residual sample was 0.594 $\pm$ 0.09 in T3D, and 0.593 $\pm$ 0.1 in T1L (95% CI), with no clear effect of MOI. Thus, the MOI accounting for infection was approximately 40% of that added to the cells. Adjusting the Poisson expectations based on this information did not change the overall conclusion that the measured infection of all viruses was markedly lower than the expectation (Fig. 5A). This result suggests that either (i) the flow cytometry assay detects only a subset of infected cells due to antigen expression levels falling below the limit of detection, or (ii) a high proportion of viruses fail to initiate productive infection, despite successful attachment to the cell monolayer. We favor the former interpretation based on the observed relationship between MOI and total viral output at 24 h postinoculation: although the detected proportion of cells infected increases very gradually over the low MOI range, viral yield increases rapidly (Fig. 5B).

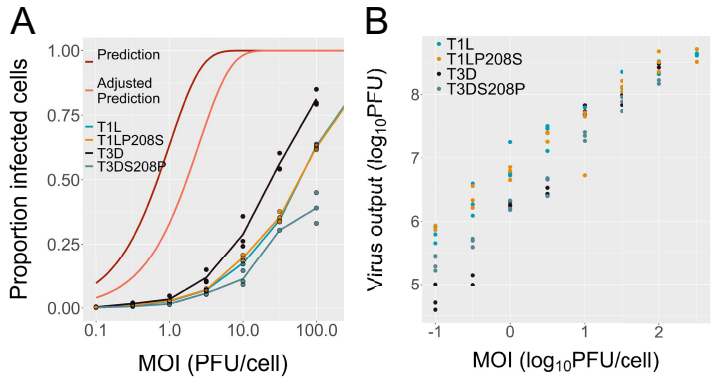

FIG 5 Flow cytometry-based detection of reovirus-positive cells appears to underrepresent levels of infection. The infectivity of T3D, T3DS208P, T1L, and T1LP208S viruses was measured using flow cytometry targeting σ3. (A) The proportion of cells expressing viral antigen was plotted against MOI. Predicted infection levels were determined based on the Poisson distribution, considering the intended MOI (Prediction) and the adjusted MOI based on the amount of inoculum virus recovered in washes (Adjusted Prediction). (B) Viral yield from *wt-var* coinfections was plotted against MOI.

For this reason, we did not generate predictions of reassortment frequency based on measured proportions of infected cells.

Disruption of microtubules does not impact reovirus genetic exchange. To further investigate the role of inclusions in defining reassortment potential, we treated infected cells with nocodazole, which disrupts the microtubule network and has been shown to inhibit inclusion body fusion (22). Nocodazole was added to uninfected L929 cells and cells infected with T3D and T3DS208P at 6 hpi. Microtubules in uninfected cells and inclusions in infected cells were visualized by confocal microscopy (Fig. 6A). Microtubules in nocodazole treated cells were noticeably disrupted, losing their linear appearance. The addition of nocodazole to infected cells resulted in small, dispersed inclusions in both T3D- and T3DS208P-infected cells at 21 hpi, as expected under conditions where inclusion merging is inhibited (22). To test the contribution of inclusion merging to reassortment, we then quantified reassortment in the presence of nocodazole (Fig. 6B and C). These results show that addition of nocodazole minimally impacted reassortment efficiency in both T3D and T3DS208P. Comparison of reassortment values at each MOI resulted in nonsignificant *P* values, ranging from 0.16 to 0.99 in T3D and from 0.12 to 0.99 in T3DS208P (Sidak's multiple-comparison test). We conclude that inclusion merging was not required for reassortment regardless of inclusion morphology.

DISCUSSION

Our results show that reovirus reassortment occurs readily in coinfected cells, with efficient assortment of all 10 gene segments observed under conditions conducive to cellular coinfection. Alteration of inclusion morphology did not affect reassortment frequencies in either T1L or T3D backgrounds, indicating that reassortment efficiency is not dependent on inclusion morphology. Furthermore, the addition of nocodazole, which has been shown to inhibit the fusion of inclusion bodies and resulted in the formation of small, dispersed inclusions in our experiments, did not result in decreased reassortment. Coalescence of inclusions may therefore not be required for genetic exchange between coinfecting reoviruses.

Previous studies using temperature-sensitive T3D mutant viruses provided clear evidence that reovirus gene segments can reassort, allowing reconstitution of a wild-type genotype from parental viruses which carried distinct temperature-sensitive mutations on differing segments. These studies could also be interpreted quantitatively and showed that wild type (that is, nontemperature-sensitive) progeny viruses occurred with a frequency of 3 to 8% when coinfections were carried out at MOIs ranging from 0.1 to 100 PFU/cell (29, 30). Importantly, these results relied on quantification of reassortment

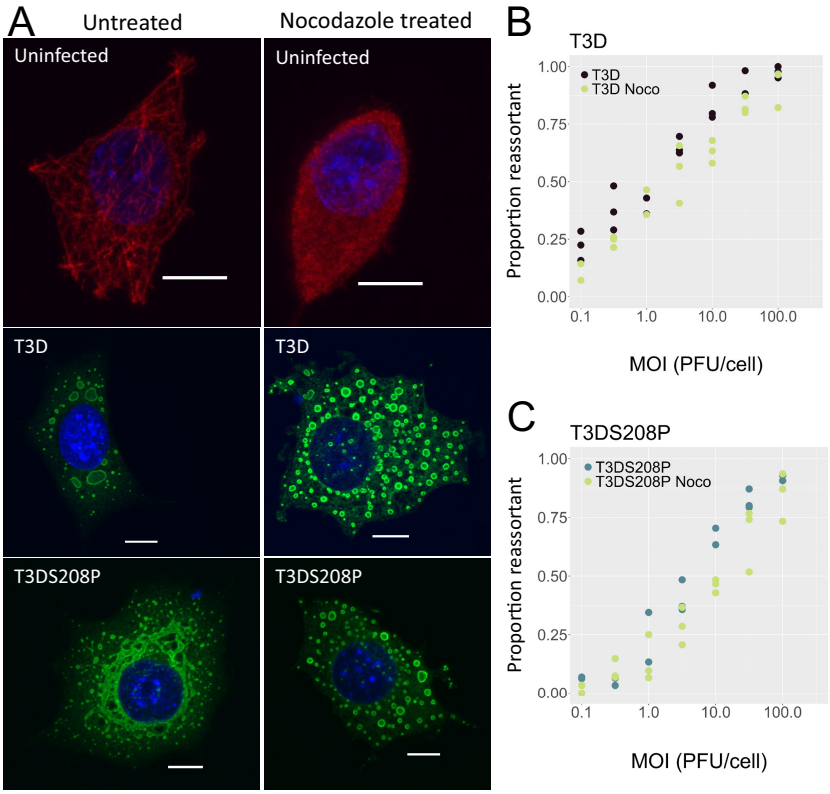

FIG 6 Treatment of cells with nocodazole does not impact reassortment. (A) Top row: Microtubules (red) and nuclei (blue) were visualized in untreated cells (left) and in cells treated with nocodazole (right). Middle and bottom rows: viral inclusions were visualized in untreated cells (left) and in cells treated with nocodazole (right), with staining for nuclei (blue) and viral σNS protein (green). Viruses used are indicated with labels overlaid on the images. Projections from a Z-stack are shown. Scale bars, 10 μm. (B, C) Reassortment was quantified for both T3D and T3DS208P viruses in the presence of nocodazole. Coinfections were performed in triplicate. Some data points are not visible due to overlap. These results are compared to reassortment frequencies without nocodazole, also reported in Fig. 2 and 3.

between only the two temperature-sensitive segments. Extrapolating these findings to consider reassortment involving any of the 10 segments yields an estimate of 6 to 16% reassortment. By comparison, our results indicate that T3D reassortment is more efficient, with as many as 25 to 100% of progeny bearing reassortant genomes. Reasons for this difference are not clear, since the same virus serotype and cell line were used and both approaches relied on genotyping of plaque isolates. It is possible that divergence of cell lines or viruses over time in culture contributes to the differing outcomes (31, 32) or that unrecognized properties of the ts mutant viruses modulated levels of coinfection or reassortment relative to those achieved here with *wt* and *var* virus pairings.

Equivalent quantification of reassortment in T1L (which has not been previously evaluated) revealed a disparity in reassortment between the serotypes. When comparing reassortment levels to mathematical predictions that assume free mixing of segments within cells and random distribution of infecting viruses, T3D reached predicted levels of reassortment while T1L remained below expectations. These differences between the serotypes were not explained by inclusion body morphology. Serotype-specific differences in cellular responses to infection, primarily in activation of cell-intrinsic antiviral responses and induction of cell death, have been observed. Compared to T1L, T3D is a more potent activator of type I interferons (33), and more frequently causes cell death by both apoptosis and necroptosis (34, 35). Infection with T3D also results in more frequent arrest of infected cells in the $_{G2}$/M phase of the cell cycle (36). It is unclear whether the differences in reassortment relate to these known variations in reovirus interactions with the host cell, or whether they are due to as-yet unknown features of the virus' biology.

In influenza A virus, high levels of reassortment result from a reliance of the virus on multiple infection for productive replication (5–7): owing to the prevalence of incomplete viral genomes, the probability of a cell producing viral progeny increases with the number of coinfecting viruses, which in turn augments the proportion of progeny viruses that are reassortant. Our results give insight into whether reovirus has a similar reliance on multiple infection. Fig. 2 indicates that reovirus reassortment is consistent with (T3D) or below (T1L) our model predictions. This model assumes a linear relationship between viral input and viral output; no synergistic effect of coinfection is incorporated. As such, our data suggest that a reliance on multiple infection for productive replication is unlikely to apply in the reovirus system. Extending this logic, our results suggest that cells infected by even a single reovirus particle typically support replication of all 10 gene segments.

Levels of reassortment are also reliant on the distribution of viruses into target cells. The simple model presented herein assumes a random, Poisson distribution and our data are generally consistent with this assumption. Delivery of multiple virus particles to a cell through various mechanisms of collective dissemination would be expected to increase reassortment (assuming the collectives include a mixture of *wt* and *var* particles). For example, reovirus aggregation (37–40), delivery of multiple virions inside extracellular vesicles (observed in rotavirus [41]), or scaffolding of multiple virions onto bacterial components (42, 43) could facilitate coinfection. While observed levels of infection in our experiments were lower than the Poisson expectation based on MOI, the shape of the infection curve was consistent with a random distribution. Additionally, the infection conditions employed in our experiments, using gradient-purified viruses, did not favor collective virus dissemination. Finally, the levels of reassortment observed either approximate (T3D) or are somewhat lower than (T1L) those predicted by our model, whereas collective dissemination would be expected to promote cellular coinfection and thus increase reassortment. Therefore, our data indicate that viral aggregates or other groupings were not a major factor driving reassortment in our experiments.

We hypothesized that inclusion coalescence was an important source of genetic mixing that led to the high levels of reassortment observed. Coalescence has been observed in the reovirus system (22), and can result in the formation of mixed inclusion bodies containing protein from both viruses (23). Blocking the merging of mature inclusions by disrupting microtubules with nocodazole presented a tractable way to test the impact of merging on reassortment. While large inclusions did not form, suggesting a lack of merging, reassortment levels were unchanged. We therefore conclude that merging of mature inclusions is not required for genetic exchange and suggest that segments may be exchanged either as a result of viral mRNA transport through the cytoplasm or prior to the formation of inclusion bodies. The latter possibility would involve assortment of primary transcripts. Primary transcription by endocytosed virions is the first biosynthetic event of the reovirus life cycle and is detected as early as 2 hpi (44–46). Newly assembled viral cores begin producing mRNA at 4 to 6 hpi and are responsible for production of the majority of viral transcripts (47, 48). It is possible that exchange of primary transcripts occurs during the formation of transcriptionally active core particles, prior to compartmentalization within viral inclusions. This model is consistent with our data in that exchange would be independent of inclusion morphology or merging.

Taken together, our data show that reovirus reassortment is more efficient than expected from the compartmentalized nature of its replication and this compartmentalization may not substantially influence reassortment frequency. Thus, the potential for reassortment to drive reovirus evolution is not markedly limited by barriers acting within the cell. Rather, reovirus genome segmentation affords ample opportunity for genetic exchange within coinfected cells.

MATERIALS AND METHODS

Experimental methods. *Viruses and Cells.* Spinner-adapted L929 cells (Terry Dermody, University of Pittsburgh) were grown at 37°C in Joklik's modified MEM supplemented with 5% FBS, 2 mM L-glutamine, penicillin, and streptomycin (PS), and 0.25 mg/mL amphotericin B; this was termed SMEM. BHK-T7 cells

(49) were maintained in DMEM supplemented with 5% FBS, 2 mM L-glutamine, PS, and 1 mg/mL G418 at 37°C. Cells were tested monthly for mycoplasma and discarded if found to be positive.

Parental T1L (accession no. SRX6802328) and T3D (accession no. SRX6802327) viruses were generated by reverse genetics (50) and were deep sequenced previously (51). Variant (*var*) T1L and T3D viruses were designed as described previously (24). As previously reported, point mutations to generate T3D *var* were: L1 C612T, L2 C853T, L3 G481A, M1 C919T, M2 A650G, M3 T702C, S1 G312A, S2 A438G, S3 T318C, and S4 C383T. Point mutations to generate T1L *var* were: L1 T606C, L2 T852C, L3 A481G, M1 T919C, M2 G650A, M3 C702T, S1 A313G, S2 C426T, S3 C318T, and S4 T383C. Additional point mutations were made at nucleotide 635 in the M1 segment (T1L C635T, T3D T635C) of both serotypes to alter inclusion morphology as shown previously (9). These viruses were generated by reverse genetics in BHK-T7 cells and propagated in L929 cells for three passages prior to Vertrel XF extraction and purification on a cesium chloride gradient (52).

Viral replication kinetics. L929 cells were infected with purified *wt* and *var* viruses of the T1L and T3D serotypes using synchronized, single-cycle conditions. At the time of infection, cells were placed on ice and washed once with 1× phosphate-buffered saline (PBS). A 100-μL volume of virus inoculum in OPTI-MEM at an MOI of 10 PFU/cell was added to each well. Cells were placed at 4°C and virus was attached for 1 h, rocking every 10 min. Keeping cells cold ensured that virus infection is synchronized, with all attached viruses entering cells simultaneously upon warming. After attachment, cells were placed back on ice and washed 3 times with cold 1× PBS. Warm SMEM was added to cells which were then placed at 37°C. At each time point, one plate was removed from incubation and stored at −80°C. At 4 hpi, warm SMEM containing 20 mM NH_4Cl (T3D) (24) or 4 mM E64-d protease inhibitor (T1L) was added to each well in order to limit further rounds of replication. Samples were titered by plaque assay on L929 cells as described previously (53).

Coinfections. Coinfections were performed using single-cycle conditions as described above. A 100-μL volume of an equal-parts mixture of *wt* and *var* viruses in OPTI-MEM was added to cells seeded in 12-well dishes at a range of MOIs. Cells were incubated for 24 h in 1 mL SMEM. Warm SMEM containing 4 mM E64D was added to T3D infections at 4 hpi and to T1L infections at 7 hpi. To determine the impact of nocodazole on reassortment, 10 μM nocodazole was added to wells infected with T3D viruses at 6 hpi. Coinfection plates were placed directly at −80°C for 3× freeze-thaw cycles. Well contents were transferred to 1.5-mL Eppendorf tubes and stored at −80°C.

Flow cytometry to quantify infected cells. Cells were harvested from 12-well plates by the addition of 100 μL trypsin (Corning) and, once they were detached, 900 μL of FACS buffer (1× PBS with 2% FBS). Cells were transferred to 1.5-mL tubes on ice and washed twice in FACS buffer. Fixation, permeabilization, and staining were performed according to the BD Cytofix/Cytoperm protocol. A 15-minute blocking step using BD rat anti-mouse CD16/CD32 Fc block was included. Infected cells were stained with a mouse monoclonal anti-σ3 antibody (clone 10C1) at a concentration of 1 μg/mL for 30 min at 4°C. Cells were washed twice, and an Alexa Fluor-647 conjugated donkey anti-mouse secondary antibody (Invitrogen) was added at a 1:1000 dilution. Cells were washed three more times and then resuspended in FACS buffer for analysis.

Data were collected on a BD LSR II Flow cytometer running FacsDiva software. A minimum of 50,000 events was collected for each sample. Analysis and gating were performed using FlowJo (v10.1). A gate was included to select single cells. Further gating selected infected cells based on positivity greater than that of an antibody stained, mock-infected control.

Wash titers. A dedicated set of infections was performed to determine the amount of virus that did not attach during coinfections and was subsequently washed away. L929 cells seeded in 6-well dishes were infected at MOIs of 0.1, 1.0, 10, and 100 PFU/cell following the synchronization protocol noted above. The supernatant was collected and pooled with 3 × 200 μL washes of cold 1× PBS. Pooled supernatant and washes were titered using a plaque assay, and the percentage of virus lost during attachment was determined based on the formula input virus (MOI × number of cells infected).

Quantification of reassortment. To obtain clonal isolates, plaque assays were performed in L929 cells with supernatant from *wt*/*var* coinfections. Well-separated plaques were picked into 120 μL of PBS in 96-well assay blocks. A total of 32 plaques were picked for each sample at each MOI. Samples were stored at −20°C or used immediately for RNA extraction.

RNA extraction was performed using the Zymo *Quick*-RNA Viral Kit I-96-well format RNA extraction kit according to the manufacturer's protocol. RNA was eluted in 40 μL water into a MicroAmp Optical 96-well reaction plate (Applied Biosystems, catalog no. N8010560).

Reverse transcription was performed in 96-well plates using Maxima reverse transcriptase (Fermentas), random hexamer primers (Thermo Fisher), and 12.8 μL of extracted RNA template.

qPCR was performed in 385-well plates (Bio-Rad, catalog no. HSP3805). A 3-μL volume of a master mix containing 1× Precision Melt Supermix (Bio-Rad) and 0.4 μM of a mixture of forward and reverse primers was mixed with 2 μL of cDNA for a total reaction volume of 5 μL. qPCR results were analyzed using Bio-Rad CFX Manager software, and melt curves were analyzed using Bio-Rad Precision Melt Analysis software.

Immunofluorescence. To analyze viral inclusion morphology, infected cells were visualized using immunofluorescence and confocal microscopy.

L929 cells were seeded onto Nunc Lab-Tek II single chambered slides (Thermo Fisher) coated with human placenta collagen. The next day, cells were infected with virus at an MOI of 5 PFU/cell. Nocodazole validation was performed using synchronized, multicycle conditions (attachment at 4°C, no E64D added) and filamentous/globular inclusion morphologies were validated using single-cycle conditions noted in the *Viral replication kinetics* section.

At 20 hpi (nocodazole) and 18 hpi (inclusion morphology), cells were washed 3 times with 1× PBS and fixed for 15 min at room temperature with 4% paraformaldehyde. Fixed cells were washed 3 more times with 1× PBS and permeabilized for 10 min with 0.2% Triton X-100 in 1× PBS. Cells were blocked for 30 min with block buffer (1× PBS with 0.1% Tween 20 and 1% bovine serum albumin [BSA]), then guinea pig anti-σNS polyclonal antibody (gift from Bernardo Mainou) at a 1:5,000 dilution in 1% BSA in 1× PBS was added to cells and allowed to incubate for 2 h at room temperature. To visualize microtubules, rabbit anti-alpha tubulin polyclonal antibody (Thermo Fisher, catalog no. 11224-1-AP) was added to cells at a 1:200 dilution in 1% BSA in 1× PBS and allowed to incubate for 2 h at room temperature. Cells were washed 3 times in 1× PBS, and Alexa Fluor 488-conjugated goat anti-guinea pig IgG H+L (Jackson ImmunoResearch, catalog no. 106-545-003) was added at a 1:2,500 dilution in 1% BSA in 1× PBS and incubated for 1 h at room temperature.

Cells were washed three times in 1× PBS, and 4 mM DAPI diluted in nuclease free water was added to cells, which were then incubated for 4 min. Cells were washed 3 more times in 1× PBS and mounted with VectaShield mounting medium.

Cells were visualized using an Olympus FV1000 Inverted Confocal Microscope with an Olympus Plan Apo 100× 1.45 NA lens. DAPI fluorophore was excited using the 405 laser, and Alexa-488 fluorophore was excited using the 488 laser line from an Argon laser. Kalman averaging was employed to reduce noise. Images were obtained using the Olympus Fluoview v4.2 software. Z-series optical sections were collected, with 13 to 24 slices at thicknesses ranging from 0.3 μM to 0.6 μM.

Computational methods. *Estimating the expected proportion of infected cells.* The expected proportion of infected cells at a given multiplicity of infection (MOI) was determined using a Poisson distribution and the following equation:

$$\text{Proportion of infected cells} = 1 - e^{-\lambda}$$

Here, λ represents the mean of the distribution and is equal to MOI.

Input versus output relationship. The observed relationship between viral input and output appears linear (Fig. 5B). As such, we let the number of output viral progeny from a cell infected with *i* virions be given by the following formula:

$$c(i) = k \times i$$

Here, *k* is the number of viral progeny produced by a virion that has entered a cell. The total viral output from a population of *N* cells is then determined using the following formula:

$$\nu(i) = \sum_i [P(i) \times c(i) \times N]$$

P(i), the probability that a cell has undergone entry of *i* virions, is given by a Poisson distribution parameterized with mean given by the MOI λ, evaluated at *i*.

Reassortment prediction. To model reassortment, the virus population must be split into two groups which are capable of coinfection. Reassortment requires coinfection to occur, and splitting the population into wild-type and variant viruses allows for this requirement to be taken into account.

The total number of virus particles that are produced at MOI λ is determined by multiplying the sum of the probabilities of *i* and *j* wild-type and variant viruses entering a cell, respectively, by the predetermined input/output relationship.

$$\sum_i \sum_j P(i)P(j)\nu(i+j)$$

Probabilities *P*(*i*) and *P*(*j*) were determined using Poisson expectations above.

To calculate the number of reassortant viruses, we first can write out the probability that a progeny virus from a cell will be reassortant if *i wt* and *j var* virions entered the cell. With the probability that a progeny virus will have all 10 gene segments be *wt* being given by $(i/[i+j])^{10}$ and the probability that a progeny virus will have all 10 gene segments be *var* being given by $(j/[i\_j])^{10}$, the probability that a progeny virus will be a reassortant genotype is given by the following formula:

$$\left[1 - \left(\frac{i}{i+j}\right)^{10} - \left(\frac{j}{i+j}\right)^{10}\right]$$

The final form of the equation to calculate the proportion of reassortant progeny is the number of reassortant viruses divided by the total number of viruses that emerge from the infection:

$$\frac{\sum_i \sum_j P(i)P(j)\left[1 - \left(\frac{i}{i+j}\right)^{10} - \left(\frac{j}{i+j}\right)^{10}\right]\nu(i+j)}{\sum_i \sum_j P(i)P(j)\nu(i+j)}$$

Analysis of pairwise associations between segments. To quantify nonrandom association of *wt* and *var*

segments during reassortment, the Pearson correlation coefficient was determined for each pair of segments at each MOI using the following formula:

$$r = \frac{\sum (x - m_x)(y - m_y)}{\sqrt{\sum (x - m_x)^2 \sum (y - m_y)^2}}$$

Where, summed across all progeny plaques that were genotyped in a sample, x is the genotype of the first segment in the pair of segments considered (e.g., M2; 1 = *wt*, 0 = *var*), y is the genotype of the second segment in the pair (e.g., S3; 1 = *wt* 0 = *var*), m_x is the proportion of first segments in the sample that are *wt*, and m_y is the proportion of second segments that are *wt*. Each r value was squared to convert the correlation to an r^2 measure.

Data availability. The reference sequences of the T1L segments used for reverse genetics can be found under the following NCBI accession numbers: M24734.1 (L1), AF378003.1 (L2), AF129820.1 (L3), X59945.1 (M1), AF490617.1 (M2), AF174382.1 (M3), EF494445.1 (S1), L19774.1 (S2), M14325.1 (S3), and X61586.1 (S4). Additionally, the reference sequences of the T3D segments used for reverse genetics can be found under the following NCBI accession numbers: EF494435.1 (L1), EF494436.1 (L2), EF494437.1 (L3), EF494438.1 (M1), EF494439.1 (M2), EF494440.1 (M3), EF494441.1 (S1), L19776.1 (S2), EF494443.1 (S3), and EF494444.1 (S4). All raw data supporting these findings and used to generate figures are available on Github at the following URL: https://github.com/MHockman/mammalian-orthoreovirus-reassortment. The data used in the generation of Fig. 1A, 2A, 2B, 3A, 3B, 4C, 4D, 4E, 4F, 5A, 5B, 6B, and 6C can be found in the data file.

ACKNOWLEDGMENTS

This work was funded by the National Institutes of Health through R01 AI146260. Furthermore, the project was supported in part by the Emory University Integrated Cellular Imaging Core and the Emory Flow Cytometry Core (EFCC). Both cores are part of the Emory Integrated Core Facilities (EICF) and are subsidized by the Emory University School of Medicine. Additional support was provided by the Center for Georgia Clinical & Translational Science Alliance of the National Institutes of Health under award number UL1TR002378.

The content is solely the responsibility of the authors and does not necessarily reflect the official views of the National Institutes of Health.

REFERENCES

1. Ince WL, Gueye-Mbaye A, Bennink JR, Yewdell JW. 2013. Reassortment complements spontaneous mutation in influenza A virus NP and M1 genes to accelerate adaptation to a new host. J Virol 87:4330–4338. https://doi.org/10.1128/JVI.02749-12.
2. Simon-Loriere E, Holmes EC. 2011. Why do RNA viruses recombine? Nat Rev Microbiol 9:617–626. https://doi.org/10.1038/nrmicro2614.
3. Chao L. 1997. Evolution of sex and the molecular clock in RNA viruses. Gene 205:301–308. https://doi.org/10.1016/s0378-1119(97)00405-8.
4. Chao L, Tran TT, Tran TT. 1997. The advantage of sex in the RNA virus phi6. Genetics 147:953–959. https://doi.org/10.1093/genetics/147.3.953.
5. Fonville JM, Marshall N, Tao H, Steel J, Lowen AC. 2015. Influenza virus reassortment is enhanced by semi-infectious particles but can be suppressed by defective interfering particles. PLoS Pathog 11:e1005204. https://doi.org/10.1371/journal.ppat.1005204.
6. Jacobs NT, Onuoha NO, Antia A, Steel J, Antia R, Lowen AC. 2019. Incomplete influenza A virus genomes occur frequently but are readily complemented during localized viral spread. Nat Commun 10:3526. https://doi.org/10.1038/s41467-019-11428-x.
7. Phipps KL, Ganti K, Jacobs NT, Lee CY, Carnaccini S, White MC, Manandhar M, Pickett BE, Tan GS, Ferreri LM, Perez DR, Lowen AC. 2020. Collective interactions augment influenza A virus replication in a host-dependent manner. Nat Microbiol 5:1158–1169. https://doi.org/10.1038/s41564-020-0749-2.
8. Sharpe AH, Chen LB, Fields BN. 1982. The interaction of mammalian reoviruses with the cytoskeleton of monkey kidney CV-1 cells. Virology 120:399–411. https://doi.org/10.1016/0042-6822(82)90040-x.
9. Parker JS, Broering TJ, Kim J, Higgins DE, Nibert ML. 2002. Reovirus core protein mu2 determines the filamentous morphology of viral inclusion bodies by interacting with and stabilizing microtubules. J Virol 76:4483–4496. https://doi.org/10.1128/jvi.76.9.4483-4496.2002.
10. Broering TJ, Parker JS, Joyce PL, Kim J, Nibert ML. 2002. Mammalian reovirus nonstructural protein microNS forms large inclusions and colocalizes with reovirus microtubule-associated protein micro2 in transfected cells. J Virol 76:8285–8297. https://doi.org/10.1128/jvi.76.16.8285-8297.2002.
11. Knipe DM, Howley PM. 2013. Fields virology, 6th ed. Wolters Kluwer/Lippincott Williams & Wilkins Health, Philadelphia, PA.
12. Miller CL, Broering TJ, Parker JS, Arnold MM, Nibert ML. 2003. Reovirus sigma NS protein localizes to inclusions through an association requiring the mu NS amino terminus. J Virol 77:4566–4576. https://doi.org/10.1128/jvi.77.8.4566-4576.2003.
13. Broering TJ, Kim J, Miller CL, Piggott CD, Dinoso JB, Nibert ML, Parker JS. 2004. Reovirus nonstructural protein mu NS recruits viral core surface proteins and entering core particles to factory-like inclusions. J Virol 78:1882–1892. https://doi.org/10.1128/jvi.78.4.1882-1892.2004.
14. Miller CL, Arnold MM, Broering TJ, Hastings CE, Nibert ML. 2010. Localization of mammalian orthoreovirus proteins to cytoplasmic factory-like structures via nonoverlapping regions of microNS. J Virol 84:867–882. https://doi.org/10.1128/JVI.01571-09.
15. Tenorio R, Fernandez de Castro I, Knowlton JJ, Zamora PF, Lee CH, Mainou BA, Dermody TS, Risco C. 2018. Reovirus sigmaNS and muNS proteins remodel the endoplasmic reticulum to build replication neo-organelles. mBio 9: e02153-18. https://doi.org/10.1128/mBio.01253-18.
16. Fernandez de Castro I, Zamora PF, Ooms L, Fernandez JJ, Lai CM, Mainou BA, Dermody TS, Risco C. 2014. Reovirus forms neo-organelles for progeny particle assembly within reorganized cell membranes. mBio 5:e00931-13. https://doi.org/10.1128/mBio.00931-13.
17. Desmet EA, Anguish LJ, Parker JS. 2014. Virus-mediated compartmentalization of the host translational machinery. mBio 5:e01463-14. https://doi.org/10.1128/mBio.01463-14.
18. Guo Y, Parker JSL. 2021. The paradoxes of viral mRNA translation during mammalian orthoreovirus infection. Viruses 13:275. https://doi.org/10.3390/v13020275.
19. Shah PNM, Stanifer ML, Hohn K, Engel U, Haselmann U, Bartenschlager R, Krausslich HG, Krijnse-Locker J, Boulant S. 2017. Genome packaging of reovirus is mediated by the scaffolding property of the microtubule network. Cell Microbiol 19. https://doi.org/10.1111/cmi.12765.

20. Miller CL, Parker JS, Dinoso JB, Piggott CD, Perron MJ, Nibert ML. 2004. Increased ubiquitination and other covariant phenotypes attributed to a strain- and temperature-dependent defect of reovirus core protein mu2. J Virol 78:10291–10302. https://doi.org/10.1128/JVI.78.19.10291-10302.2004.
21. Eichwald C, Ackermann M, Nibert ML. 2018. The dynamics of both filamentous and globular mammalian reovirus viral factories rely on the microtubule network. Virology 518:77–86. https://doi.org/10.1016/j.virol.2018.02.009.
22. Bussiere LD, Choudhury P, Bellaire B, Miller CL. 2017. Characterization of a replicating mammalian orthoreovirus with tetracysteine-tagged muNS for live-cell visualization of viral factories. J Virol 91:e01371-17. https://doi.org/10.1128/JVI.01371-17.
23. Campbell EA, Reddy V, Gray AG, Wells J, Simpson J, Skinner MA, Hawes PC, Broadbent AJ. 2020. Discrete virus factories form in the cytoplasm of cells coinfected with two replication-competent tagged reporter birnaviruses that subsequently coalesce over time. J Virol 94:e02107-19. https://doi.org/10.1128/JVI.02107-19.
24. Hockman MR, Phipps KL, Holmes KE, Lowen AC. 2020. A method for the unbiased quantification of reassortment in segmented viruses. J Virol Methods 280:113878. https://doi.org/10.1016/j.jviromet.2020.113878.
25. White MC, Lowen AC. 2018. Implications of segment mismatch for influenza A virus evolution. J Gen Virol 99:3–16. https://doi.org/10.1099/jgv.0.000989.
26. Marshall N, Priyamvada L, Ende Z, Steel J, Lowen AC. 2013. Influenza virus reassortment occurs with high frequency in the absence of segment mismatch. PLoS Pathog 9:e1003421. https://doi.org/10.1371/journal.ppat.1003421.
27. Wittwer CT, Reed GH, Gundry CN, Vandersteen JG, Pryor RJ. 2003. High-resolution genotyping by amplicon melting analysis using LCGreen. Clin Chem 49:853–860. https://doi.org/10.1373/49.6.853.
28. Cross RK, Fields BN. 1976. Use of an aberrant polypeptide as a marker in three-factor crosses: further evidence for independent reassortment as the mechanism of recombination between temperature-sensitive mutants of reovirus type 3. Virology 74:345–362. https://doi.org/10.1016/0042-6822(76)90341-x.
29. Spandidos DA, Graham AF. 1976. Recombination between temperature-sensitive and deletion mutants of reovirus. J Virol 18:117–123. https://doi.org/10.1128/JVI.18.1.117-123.1976.
30. Fields BN. 1971. Temperature-sensitive mutants of reovirus type 3 features of genetic recombination. Virology 46:142–148. https://doi.org/10.1016/0042-6822(71)90013-4.
31. Mohamed A, Clements DR, Gujar SA, Lee PW, Smiley JR, Shmulevitz M. 2020. Single amino acid differences between closely related reovirus T3D lab strains alter oncolytic potency *in vitro* and *in vivo*. J Virol 94:e01688-19. https://doi.org/10.1128/JVI.01688-19.
32. Mohamed A, Konda P, Eaton HE, Gujar S, Smiley JR, Shmulevitz M. 2020. Closely related reovirus lab strains induce opposite expression of RIG-I/IFN-dependent versus -independent host genes, via mechanisms of slow replication versus polymorphisms in dsRNA binding sigma3 respectively. PLoS Pathog 16:e1008803. https://doi.org/10.1371/journal.ppat.1008803.
33. Stuart JD, Holm GH, Boehme KW. 2018. Differential delivery of genomic double-stranded RNA causes reovirus strain-specific differences in interferon regulatory factor 3 activation. J Virol 92:e01947-17. https://doi.org/10.1128/JVI.01947-17.
34. Tyler KL, Squier MK, Rodgers SE, Schneider BE, Oberhaus SM, Grdina TA, Cohen JJ, Dermody TS. 1995. Differences in the capacity of reovirus strains to induce apoptosis are determined by the viral attachment protein sigma 1. J Virol 69:6972–6979. https://doi.org/10.1128/JVI.69.11.6972-6979.1995.
35. Berger AK, Danthi P. 2013. Reovirus activates a caspase-independent cell death pathway. mBio 4:e00178-13. https://doi.org/10.1128/mBio.00178-13.
36. Poggioli GJ, Keefer C, Connolly JL, Dermody TS, Tyler KL. 2000. Reovirus-induced G(2)/M cell cycle arrest requires sigma1s and occurs in the absence of apoptosis. J Virol 74:9562–9570. https://doi.org/10.1128/jvi.74.20.9562-9570.2000.
37. Floyd R, Sharp DG. 1978. Viral aggregation: quantitation and kinetics of the aggregation of poliovirus and reovirus. Appl Environ Microbiol 35:1079–1083. https://doi.org/10.1128/aem.35.6.1079-1083.1978.
38. Floyd R, Sharp DG. 1978. Viral aggregation: effects of salts on the aggregation of poliovirus and reovirus at low pH. Appl Environ Microbiol 35:1084–1094. https://doi.org/10.1128/aem.35.6.1084-1094.1978.
39. Floyd R, Sharp DG. 1977. Aggregation of poliovirus and reovirus by dilution in water. Appl Environ Microbiol 33:159–167. https://doi.org/10.1128/aem.33.1.159-167.1977.
40. Floyd R, Sharp DG. 1979. Viral aggregation: buffer effects in the aggregation of poliovirus and reovirus at low and high pH. Appl Environ Microbiol 38:395–401. https://doi.org/10.1128/aem.38.3.395-401.1979.
41. Santiana M, Ghosh S, Ho BA, Rajasekaran V, Du WL, Mutsafi Y, De Jesus-Diaz DA, Sosnovtsev SV, Levenson EA, Parra GI, Takvorian PM, Cali A, Bleck C, Vlasova AN, Saif LJ, Patton JT, Lopalco P, Corcelli A, Green KY, Altan-Bonnet N. 2018. Vesicle-cloaked virus clusters are optimal units for inter-organismal viral transmission. Cell Host Microbe 24:208–220.e8. https://doi.org/10.1016/j.chom.2018.07.006.
42. Kuss SK, Best GT, Etheredge CA, Pruijssers AJ, Frierson JM, Hooper LV, Dermody TS, Pfeiffer JK. 2011. Intestinal microbiota promote enteric virus replication and systemic pathogenesis. Science 334:249–252. https://doi.org/10.1126/science.1211057.
43. Berger AK, Yi H, Kearns DB, Mainou BA. 2017. Bacteria and bacterial envelope components enhance mammalian reovirus thermostability. PLoS Pathog 13:e1006768. https://doi.org/10.1371/journal.ppat.1006768.
44. Jacobs BL, Atwater JA, Munemitsu SM, Samuel CE. 1985. Biosynthesis of reovirus-specified polypeptides. The s1 mRNA synthesized *in vivo* is structurally and functionally indistinguishable from *in vitro*-synthesized s1 mRNA and encodes two polypeptides, sigma 1a and sigma 1bNS. Virology 147:9–18. https://doi.org/10.1016/0042-6822(85)90222-3.
45. Silverstein SC, Dales S. 1968. The penetration of reovirus RNA and initiation of its genetic function in L-strain fibroblasts. J Cell Biol 36:197–230. https://doi.org/10.1083/jcb.36.1.197.
46. Zweerink HJ, Joklik WK. 1970. Studies on the intracellular synthesis of reovirus-specified proteins. Virology 41:501–518. https://doi.org/10.1016/0042-6822(70)90171-6.
47. Ito Y, Joklik WK. 1972. Temperature-sensitive mutants of reovirus: I. Patterns of gene expression by mutants of groups C, D, and E. Virology 50:189–201. https://doi.org/10.1016/0042-6822(72)90359-5.
48. Lemay G. 1988. Transcriptional and translational events during reovirus infection. Biochem Cell Biol 66:803–812. https://doi.org/10.1139/o88-092.
49. Buchholz UJ, Finke S, Conzelmann KK. 1999. Generation of bovine respiratory syncytial virus (BRSV) from cDNA: BRSV NS2 is not essential for virus replication in tissue culture, and the human RSV leader region acts as a functional BRSV genome promoter. J Virol 73:251–259. https://doi.org/10.1128/JVI.73.1.251-259.1999.
50. Kobayashi T, Antar AA, Boehme KW, Danthi P, Eby EA, Guglielmi KM, Holm GH, Johnson EM, Maginnis MS, Naik S, Skelton WB, Wetzel JD, Wilson GJ, Chappell JD, Dermody TS. 2007. A plasmid-based reverse genetics system for animal double-stranded RNA viruses. Cell Host Microbe 1:147–157. https://doi.org/10.1016/j.chom.2007.03.003.
51. Rodriguez Stewart RM, Berry JTL, Berger AK, Yoon SB, Hirsch AL, Guberman JA, Patel NB, Tharp GK, Bosinger SE, Mainou BA. 2019. Enhanced killing of triple-negative breast cancer cells by reassortant reovirus and topoisomerase inhibitors. J Virol 93:e01411-19. https://doi.org/10.1128/JVI.01411-19.
52. Furlong DB, Nibert ML, Fields BN. 1988. Sigma 1 protein of mammalian reoviruses extends from the surfaces of viral particles. J Virol 62:246–256. https://doi.org/10.1128/JVI.62.1.246-256.1988.
53. Virgin HWt, Bassel-Duby R, Fields BN, Tyler KL. 1988. Antibody protects against lethal infection with the neurally spreading reovirus type 3 (Dearing). J Virol 62:4594–4604. https://doi.org/10.1128/JVI.62.12.4594-4604.1988.